AEGC Australasian Exploration Geoscience Conference Brisbane 2021

Simultaneous inversion of teleseismic P- and converted S-waves to constrain the seismic structure of the crust

Mehdi Tork Qashqai
Deep Earth Imaging
Future Science Platform
CSIRO Energy
Kensington, WA, Australia
Mehdi.Torkqashqai@csiro.au

Erdinc Saygin
Deep Earth Imaging
Future Science Platform
CSIRO Energy
Kensington, WA, Australia
Erdinc.Saygin@csiro.au

SUMMARY

Traveltimes of P and mode-converted S-waves and their reverberations place a tight constraint on the Vp/Vs ratio and their amplitude ratio provides tight bounds on the P and S wave velocity jumps across the main discontinuities in the subsurface structure below a seismic receiver. Seismic P-to-S converted waves have been used for decades to estimate the shear-wave velocity of the subsurface and depths of major discontinuities below a seismic receiver through a method known as the P wave receiver functions. Here, a new and alternative approach is presented using P and all mode-converted shear waves in a probabilistic joint inversion framework to simultaneously estimate seismic properties of the crust (Vp, Vs, and Vp/Vs). These waves are extracted by the autocorrelation of the teleseismic P-wave coda recorded on the radial and vertical component of a three-component (3C) seismic receiver. In the application of the methodology, we image the crust along a north-south oriented passive seismic line (BILBY) in central Australia, which traverses multiple geological domains. The overall trend of our inferred Moho follows the long-wavelength pattern of the Moho interpreted from the deep seismic reflection line-GOMA parallel to the BILBY experiment. It is also consistent with the reflectivity changes seen at the base of the crust in the GOMA seismic section. Our approach is a cost-effective method and can be used in conjunction with the deep active seismic reflection profiling to obtain additional information, especially at depths where the deep seismic reflection method cannot image.

Key words: joint inversion, autocorrelation, teleseismic P-wave coda, crustal structure, central Australia

INTRODUCTION

P-wave energy from a direct teleseismic source converts to S energy and vice versa across a sharp seismic boundary beneath a seismic station. This incoming energy contains multiple reflections from the underlying structure as well as peg-leg multiples and scattered and mode converted waves (coda). Teleseismic waves recorded on the vertical and radial components of a seismogram have been widely used to retrieve the impulse response of the receiver-side structure by deconvolving the vertical component (P) from the horizontal or radial component (S). The resulting waveform is primarily sensitive to sharp Vs changes with depth and is commonly referred to as the "P wave receiver function" (hereafter RF), which represents the converted P- to S-wave energy directly beneath a seismic station (Ammon, 1991; Langston, 1979). In addition to the RFs, single station autocorrelation of teleseismic records can provide complementary constraints on the crustal properties beneath a seismic station. Compared to the RFs, the autocorrelations of the teleseismic P-wave coda include both P- and P-to-S converted phases, whereas the RFs contain P-to-S phases primarily because the P-waves are cancelled by the deconvolution operation in the RFs (Figure 1). Thus, both Vp and Vs can simultaneously be estimated by jointly inverting the radial and vertical components' autocorrelations. Such a joint inversion approach offers a framework to reduce further the uncertainties associated with the crustal seismic properties (Vp, Vs and Vp/Vs), and thus can provide an improved estimate of both Vp and Vs, and consequently the Vp/Vs ratio, which provides an indication of the rock lithology beneath a seismic station. In this study, we image the crust beneath central Australia along a north-south seismic profile (BILBY seismic array) through the probabilistic joint inversion of radial and vertical components' autocorrelations of the teleseismic P-wave coda and compare our results with the results obtained from RF analysis (Sippl, 2016), AusMoho (Kennett. et al., 2011), the deep seismic reflection profiling (Korsch & Doublier, 2016) and the inversion of the vertical component autocorrelation (Tork Qashqai et al., 2019).

AUTOCORRELATION METHOD

In a plane-layered medium, when a steep incident plane P-wave from a distant earthquake (epicentral distances between 30° and 90°) impinges on an interface in the subsurface (e.g., Moho), the seismogram on the surface records direct P-wave energy, its direct P-to-S conversion phase, its peg-leg multiples and scattered waves including free-surface related multiples (Figure 1). The recorded teleseismic waveforms on the horizontal and vertical components of a seismogram can be processed to estimate the subsurface structure's impulse-response in the forms of autocorrelations.

Claerbout (1968) showed that for plane waves impinging at normal incidence to a horizontally stratified acoustic medium with a free surface, the positive or negative part of the autocorrelation of the acoustic transmission response corresponds to the reflection response of the Earth beneath that station. We further illustrate this in Figure 1 for a simple synthetic 1-D Earth model of one crustal layer over a half-space. The autocorrelations of the vertical or radial components of a seismometer contain seismic waves reflected from the free-surface, such as Pppmp and Ppsms (Figure 1). These reflections have the same delay times as PmP and SmS that are reflected from the bottom of the model (e.g., the Moho) and can be thought of as the Earth's response to a virtual source co-located with the at the surface of the Earth

(Figure 1). As seen from Figure 1, the autocorrelations of both the radial and vertical components not only have the P-to-S phases that exist in the RF but also contain the PmP phase and carry additional information from the subsurface. Therefore, the inverse modelling of autocorrelation waveforms provides a means of subsurface characterisation.

DATA SELECTION AND PROCESSING

In this study, we follow the approach of Tork Qashqai et al. (2019) for data selection and processing. We use teleseismic P-wave coda associated with events with Mw > 5.5 and epicentral distances between 30° and 90 ° recorded by the vertical and radial components of broadband seismic stations along the BILBY profile (Figure 2). We choose P-wave coda from a time window of 10-40 s (30 sec long) after the onset of the theoretical P-wave arrivals predicted by the ak135 model (Kennett et al., 1995). We remove the mean and trend of each record and reject bad quality records and then resample the data to 10 Hz. To retrieve approximate reflection responses for each seismic station, we apply a Butterworth band-pass filter (1st order, zero phase) in the frequency range of 1 and 2 Hz before and after the autocorrelation process, and then normalise amplitudes to unity.

Traveltimes of converted and reverberation phases (e.g., direct Ps or Pms, Pppmp, Pppms and Ppsms) in the autocorrelations of teleseismic P-wave coda are a function of the incident angle of the impinging seismic wave. The incident angle is controlled by the slowness of the primary teleseismic P-wave or the epicentral distance of the teleseismic earthquake. The travel time curves associated with the conversions and reverberations in the P-wave coda, which are originated at different depths beneath a seismic station, cannot be exactly parallel. For example, for slowness range between 0.04 and 0.08 s/km, an increase of the slowness parameter (decreasing the epicentral distance) leads to an increase of the relative arrival times of the primary P to S converted phase (Pms) and a decrease of the travel times of the Pppmp (pmp), Pppms and Ppsms (sms) phases with respect to the primary P-wave. Therefore, the moveouts of travel time curves for the converted and reverberated phases are not parallel and they need to be corrected prior to stacking. For each seismic station, both the radial and vertical components autocorrelation waveforms from multiple events are corrected for the moveouts by stretching/contracting autocorrelations with respect to the time scale of the reference autocorrelation (with slowness of 0.065 s/km). Then we stack the moveout corrected autocorrelation waveforms from multiple events to increase the signal-to-noise ratio and eliminate the source effects on reflection seismograms (Claerbout, 1968).

JOINT PROBABILISTIC INVERSION METHOD

We adopted the Delayed Rejection Adaptive Metropolis algorithm (DRAM) (Haario et al., 2006). DRAM is a Markov Chain Monte Carlo (MCMC) approach and has been widely used in many geophysical model parameter estimation problems (Ball et al., 2014; Afonso et al., 2016; Tork Qashqai et al., 2018). DR provides a mechanism for drawing alternative samples when the current sample is rejected in the standard Metropolis-Hastings algorithm (Tierney, 1994), thus improving the efficiency of the sampling by reducing the number of rejections. In the AM, to reduce the sampling of low probability areas in the model space, the algorithm updates the covariance matrix of the chain (after a non-adaptation period) using all the previously accepted samples. This process can be iterated at regular intervals. In this study, the total number of simulations per station is 400,000. The non-adaptation time includes 150,000 iterations (or samples), and the proposal distribution of the model is updated after the non-adaptation time every 3,000 samples.

1-D PARAMETERISATION AND FORWARD PROBLEM

The 1-D crust below each seismic station is parameterised with a stack of ten plane horizontal homogeneous crustal layers bounded at the base of the crust by a homogeneous upper mantle as a half-scape. We use a step function parameterisation, including ten crustal layers for joint inversion of the field data. This allows the inversion to capture the potential gradational transition across crustal discontinuities, including the crust-mantle boundary (Moho) that exist in central Australia (Kennett. et al., 2011). Each crustal layer is described by three parameters: density, thickness variation (ΔH) and Vp/Vs. Upper mantle parameters (Vp/Vs and density), as well as the slowness parameter, are considered as unknown parameters during the inversion. The slowness parameter is allowed to vary only between 0.064 and 0.066 km/s as we applied a moveout correction to the observed autocorrelations assuming a reference slowness of 0.065 s/km.

The first step in the MCMC inversion is to randomly draw values for the main unknown parameters from their prior distributions (Table 1). Note that for the perturbation of crustal thicknesses in our inversion framework, the MCMC algorithm needs an initial crustal thickness model to perturb. Here, we assume that the initial crustal thickness below each seismic station is 40 km and includes ten layers, each with an equal thickness of 4 km. To perturb the initial crustal thickness model, the initial thickness of each layer is randomly perturbed (by the MCMC algorithm) using the random value drawn in the earlier step from the range of ΔH given in Table 1. In the next step, P-wave velocities for each layer (including the half-space) are estimated from the sampled random density values using the empirical Nafe-Drake curve (Ludwig et al., 1970; Brocher, 2005). The Vs value for each layer is then calculated from the computed Vp and the Vp/Vs values drawn by the MCMC algorithm.

Given the random slowness value drawn from its prior range and the crustal parameters, the synthetic seismograms are computed using the reflectivity method of Kennett (1983) as implemented by Randall (1989). Autocorrelations of the vertical and radial components are calculated to estimate the synthetic reflection responses of the 1-D Earth beneath each station. A Butterworth band-pass filter (1st order, zero-phase) in the frequency range of 1 and 2 Hz is applied before and after the autocorrelation and amplitudes are normalised to unity.

RESULTS

Figure 3 shows an example of the results from the 1-D joint inversion for one of the stations from the BILBY experiment (BL15). The posterior distributions of the Vp/Vs ratio, Vp and Vs in the forms of density plots as well as the fits to the observed data (Figures 3a and 3b). In density plots, the high probability areas are displayed with hot colours and the blue colour represents the mean of the posterior distributions of the Vp, Vs and the Vp/Vs structures.

The mean values of the posterior distributions of the Vp, Vs and Vp/Vs associated with individual stations are interpolated to create sections of crustal properties (Figure 4) along the BILBY transect (shown by a red dashed line in Figure 2b). The crustal Vp and Vs sections (Figure 4) shows dominant low velocities at depths < 30 km along the transect whereas depths greater than 30 km mainly characterise with higher velocities. The Vp/Vs section shows a very complex pattern of high and low values. It seems that the high Vp/Vs values at depths greater than 10 km are mostly localised beneath locations where the crustal blocks interact (e.g., across the transition from one domain to another). In the middle crust of the Officer Basin and the Gawler Craton, a high-velocity layer (which has a low Vp/Vs ratio) lies between the low-velocity layers (featuring high Vp/Vs ratios). The crust beneath the Musgrave Province, Officer Basin and Arunta Block is characterised by Moho uplifts. Moho varies between 37 km and 53 km along the BILBY transect. A distinct pattern of the Moho variation is recognisable along the transect across the transition from crustal domains. For example, the Moho is deep in the Georgina Basin and gets shallower beneath the Arunta Block. It then gets deeper towards the Amadeus Basin, uplifted in the Musgrave province and the Officer Basin.

Recently, several studies have discussed the crustal structure of central Australia using either passive seismic data recorded by the stations along the BILBY experiment (Sippl, 2016; Thompson et al., 2019), or deep seismic reflection data. Geoscience Australia conducted several deep seismic sounding profiles with 20 s recording time across Australia (Kennett & Saygin, 2015; Kennett. et al., 2016) to better map the crustal structure and geodynamic evolution of the major geological provinces of Australia. Korsch and Doublier (2016) interpreted the major crustal boundaries and Moho across several regions in Australia, including along the GOMA seismic line. We compare our Moho estimates with the Moho depths estimated from RFs (Sippl, 2016), the AusMoho model (Kennett. et al., 2011), the inversion of the only autocorrelation of the vertical component (Tork Qashqai et al., 2019) in Figure 4. In Figure 5, we compared our Moho estimates (black horizontal bars) with those interpreted from the deep seismic reflection (dark green line) method (Korsch & Doublier, 2016, GOMA line). The Moho values obtained from this study are converted to their corresponding two-way travel time using our inverted P-wave velocity model (Figure 4a).

The estimated travel times of the seismic wave reflected from the Moho in our study are mostly less than those interpreted from the active seismic reflection method which is due to a different velocity model being used to produce the migrated section. A large station interval in the passive seismic recording of the BILBY profile (lack of data between stations) and the higher spatial resolution of the deep seismic reflection line can be the reasons for this difference. In this study, the Moho values between stations (where there is a gap in recording passive seismic data) are estimated by simple interpolation. However, the general trend of our Moho model in the time domain in the south of the Amadeus Basin follows the long-wavelength pattern of Moho interpreted from the deep seismic reflection sounding along the GOMA seismic line (Figure 5). The trend of the Moho structure from the active seismic, AusMoho model (green bars in Figures 4a and 4b), and our approach beneath the Officer Basin shows southward thinning of the crust (from stations BL20 to station BL22). In contrast, to the south of station BL22, the crust thickens toward the Gawler Craton and reaches ~ 50 km below station BL23, where a crustal-scale fault has been interpreted to cut and displace the Moho (Korsch & Doublier, 2016; also see Figure 5). Below station BL21, our Moho value is closer to the change of the reflectivity at the base of the crust.

CONCLUSIONS

We introduce a new joint inversion approach to estimate Vp, Vs, and Vp/Vs ratio structures simultaneously below a seismic station utilising both the vertical and radial component autocorrelations of the teleseismic P-wave coda. We successfully applied this technique on passive seismic data recorded along a north-south transect in central Australia to image and characterise the crustal blocks and their properties (Vp, Vs, Moho and Vp/Vs ratio) simultaneously. This study provides the first comprehensive joint estimates of all crustal properties for the BILBY seismic transect. The joint inversion of the radial and vertical autocorrelations of the teleseismic P-wave coda has significant implications for characterising the Vp/Vs ratio, which is a good indicator of crustal composition. The Moho structure's overall trend along the profile is compatible with that interpreted from the migrated seismic reflection section (GOMA) and the general reflectivity character of the Moho reflection at the base of the crust. This demonstrates the feasibility of our joint inversion method to provide complementary information on the crustal structure. We note that the new joint inversion approach is more cost-effective than the deep reflection profiling method and can be used to obtain additional information about the deep Earth, especially at depths where the deep seismic reflection method cannot image.

ACKNOWLEDGMENTS

This research was funded by the Deep Earth Imaging Future Science Platform, CSIRO. Inversions were performed using the Pearcey High-Performance Computing (HPC) cluster of the Commonwealth Scientific and Industrial Research Organization (CSIRO). Seismic data were retrieved from the AusPass archive (http://auspass.edu.au/) under a Creative Commons Attribution 4.0 International license (CC BY 4.0: https://creativecommons.org/licenses/by/4.0/). The processed GOMA seismic reflection section can be downloaded from the Geoscience Australia portal (http://pid.geoscience.gov.au/dataset/ga/70579) under Creative Commons Attribution 4.0 International Licence. We thank Michael Doublier and Malcolm Nicoll from Geoscience Australia for sharing their deep seismic reflection interpretation with us.

REFERENCE

Afonso, J. C., Rawlinson, N., Yang, Y., Schutt, D. L., Jones, A. G., Fullea, J., & Griffin, W. L. (2016). 3-D multiobservable probabilistic inversion for the compositional and thermal structure of the lithosphere and upper mantle: III. Thermochemical tomography in the western-central U.S. Journal of Geophysical Research: Solid Earth, 121 (10), 7337-7370.

Ammon, C. J. (1991). The isolation of receiver effects from teleseismic P waveforms. Bulletin of the Seismological Society of America, 81 (6), 2504-2510.

Ball, J. S., Sheehan, A. F., Stachnik, J. C., Lin, F. C., & Collins, J. A. (2014). A joint Monte Carlo analysis of seafloor compliance, Rayleigh wave dispersion and receiver functions at ocean bottom seismic stations offshore New Zealand. Geochemistry, Geophysics, Geosystems, 15 (12), 5051-5068.

Brocher, T. M. (2005). Empirical Relations between Elastic Wavespeeds and Density in the Earth's Crust. Bulletin of the Seismological Society of America, 95 (6), 2081-2092.

Claerbout, J. F. (1968). Synthesis of a layered medium from its acoustic transmission response. Geophysics, 33 (2), 264-269.

Haario, H., Laine, M., Mira, A., & Saksman, E. (2006). DRAM: Efficient adaptive MCMC. Statistics and Computing, 16 (4), 339-354.

Kennett, B. L. N. (1983). Seismic wave propagation in stratified media. Cambridge: Cambridge University Press.

Kennett., B. L. N., Salmon, M., Saygin, E., & Group, A. W. (2011). AusMoho: The variation of Moho depth in Australia. Geophysical Journal International, 187 (2), 946-958.

Korsch, R. J., & Doublier, M. P. (2016). Major crustal boundaries of Australia, and their significance in mineral systems targeting. Ore Geology Reviews, 76, 211-228.

Langston, C. A. (1979). Structure under Mount Rainier, Washington, inferred from teleseismic body waves. Journal of Geophysical Research, 84 (B9), 4749-4762.

Ludwig, W. J., Nafe, J. E., & Drake, C. L. (1970). Seismic refraction, in the sea, A. E. Maxwell (editor) (Vol. 4). New York: Wiley-Interscience.

Maher, J. L. (2010). L190 Gawler-Officer-Musgrave-Amadeus Deep Crustal Seismic Survey, SA & NT, 2008. Stacked and Migrated Data and Images for 08GA-OM. Geoscience Australia, Canberra.

Randall, G. E. (1989). Efficient calculation of differential seismograms for lithospheric receiver functions. Geophysical Journal International, 99 (3), 469-481.

Sippl, C. (2016). Moho geometry along a north-south passive seismic transect through Central Australia. Tectonophysics, 676, 56-69.

Tierney, L. (1994). Markov chains for exploring posterior distributions. Ann. Statist., 22 (4), 1701-1728.

Tork Qashqai, M., Afonso, J. C., & Yang, Y. (2018). Physical state and structure of the crust beneath the western-central united states from multiobservable probabilistic inversion. Tectonics, 37 (9), 3117-3147.

Tork Qashqai, M., Saygin, E., & Kennett, B. L. N. (2019). Crustal imaging with Bayesian inversion of teleseismic P wave coda autocorrelation. Journal of Geophysical Research: Solid Earth, 124 (6), 5888-5906.

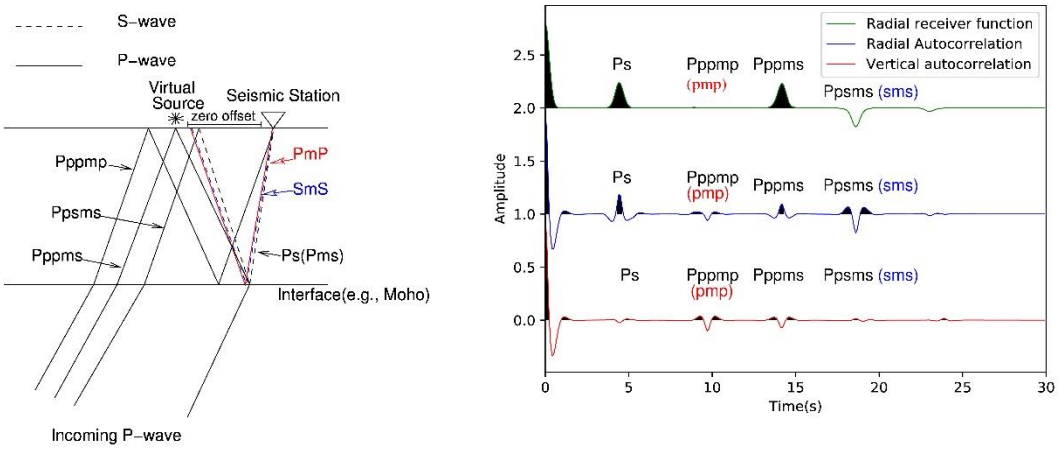

Figure 1. Left: schematic representation of a teleseismic plane wave impinging on a layer. Thickness, Vp, Vs, Vp/Vs of the layer are 35 km, 6.65 km/s, 3.69 km/s and 1.8. Note that the diagram is horizontally exaggerated to highlight the seismic phases. Right: shows the delay times of the main phases and the free-surface related multiples associated with the receiver function (top), the autocorrelation of the radial (middle) and vertical (bottom) components which were obtained using the model shown on the left. Capital P denotes the upcoming P-wave in the half-space/mantle. All the lower-case letters denote p or s waves in the crust. The lower-case p or s before and after the letter 'm' denote the P or S-waves impinge (downward wave) on and reflected (upgoing wave) from the Moho, respectively.

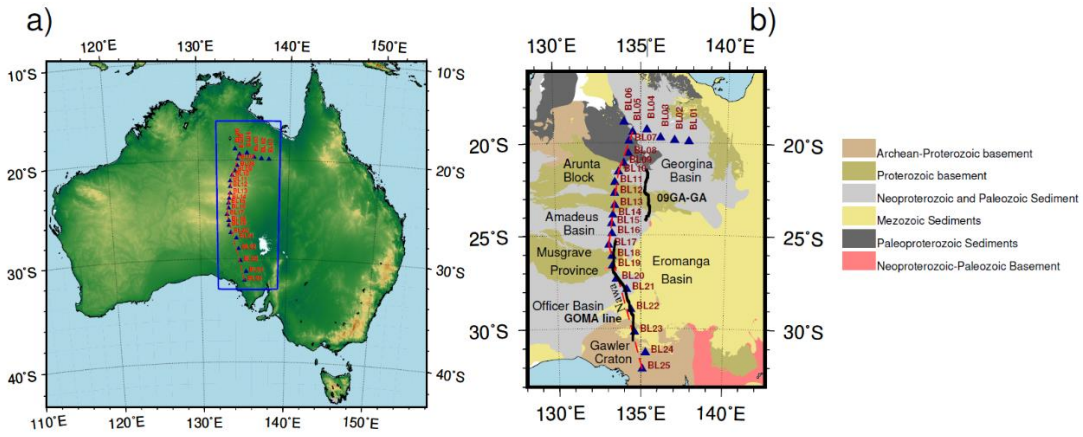

Figure 2. a) The BILBY experiment seismic stations are marked on the topographic map of Australia. The blue box shows the area shown in the right subfigure (b), where the locations of the seismic stations and the GOMA and 09GA active seismic reflection lines are superimposed on the main geological units of central Australia. The crustal properties (shown in Figure 4) are extracted along the red dashed line.

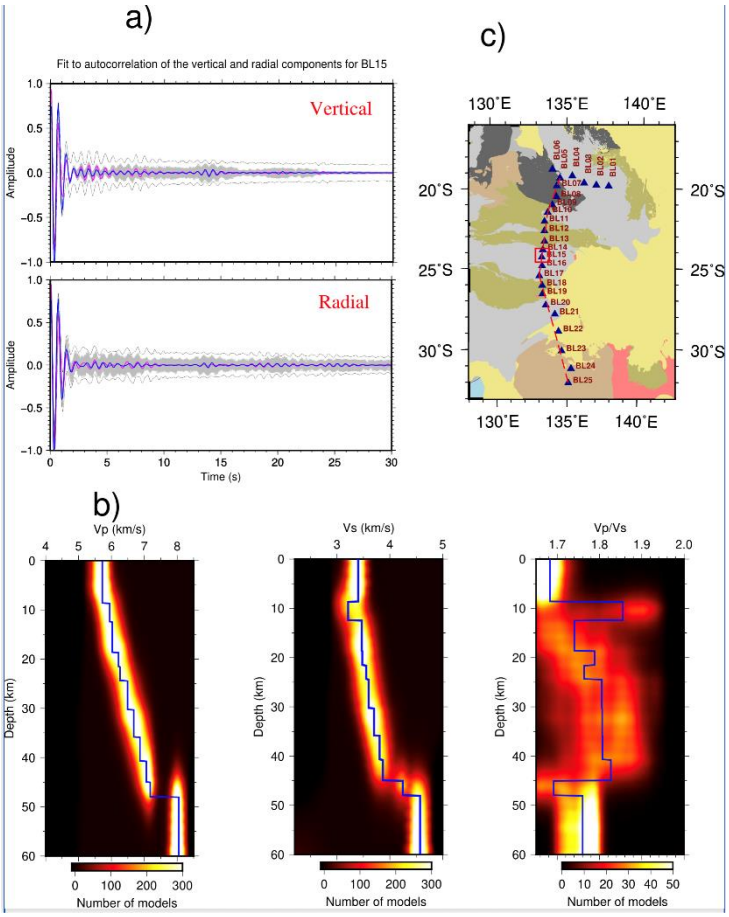

Figure 3. Results of the joint inversion of field measurements for station BL15. a) Fit to the autocorrelation of the vertical and radial components, b) Density plots of Vp, Vs and the Vp/Vs ratio, c) The location of station BL15 is highlighted with a red box on the map of the study area. In the density plots, the mean values of the best 2000 accepted models in the posterior distributions are displayed with blue colours. In plots showing the fits to autocorrelations of the radial and vertical components, red is the observed data, and blue is the mean of the best 2000 accepted predicted data (greys).

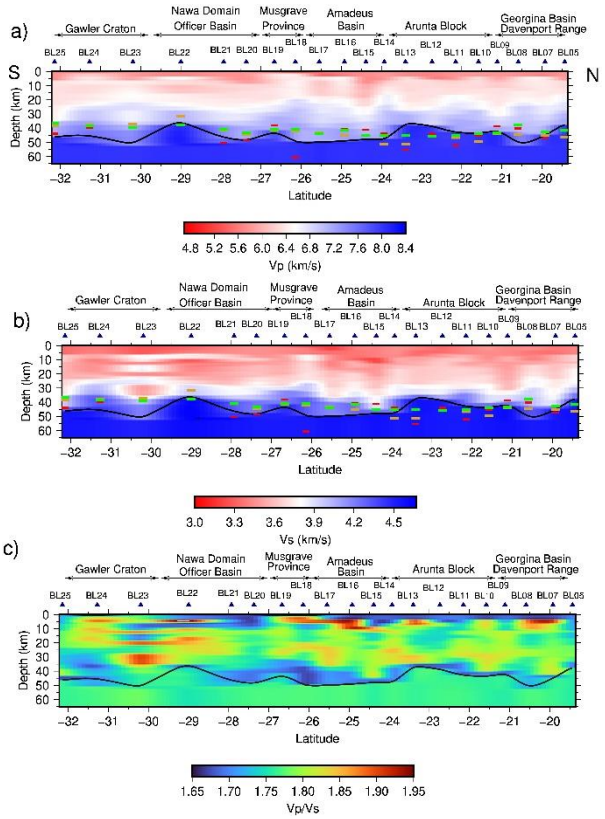

Figure 4. Sections of crustal properties inferred from combining the 1-D joint inversion results along the red transect shown in Figure 2. a) Vp, b) Vs, and c) Vp/Vs. The locations of seismic stations along the transect are marked by blue triangles. The main geological units and crustal blocks are also indicated. The Moho structure obtained in this study is shown by a black line. The Moho depth values estimated by the H-K stacking method (Sippl, 2016, red thick horizontal bars), the inversion of the vertical component autocorrelation (Tork Qashqai et al., 2019, light brown thick horizontal bars), and the AusMoho (Kennett. et al., 2011, green bars) are also plotted on the Vp and Vs sections for comparison.

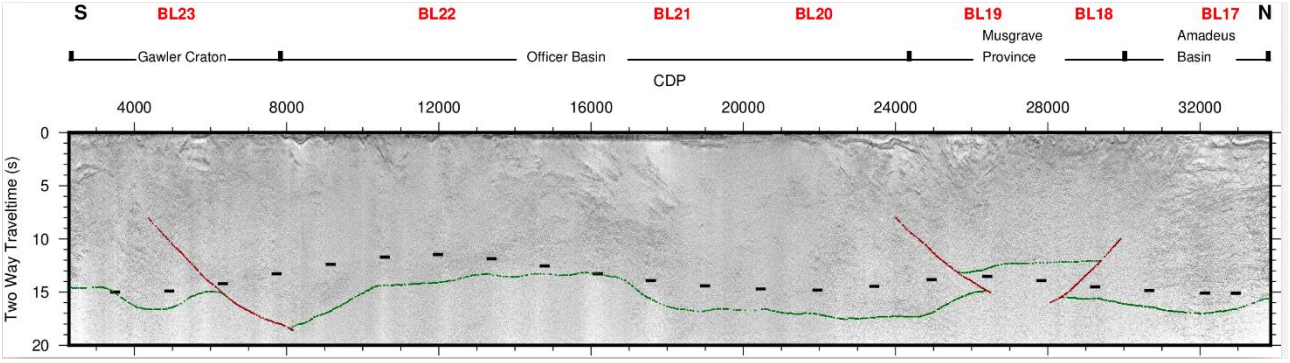

Figure 5. The Moho structure imaged by our joint inversion approach (black horizontal bars) is superimposed on the Gawler-Officer-Musgrave-Amadeus (GOMA) migrated seismic reflection section (see Figure 2 for the location of the line) taken from Geoscience Australia (Maher, 2010). The dark green structure represents the interpreted Moho from the GOMA migrated seismic section (Korsch & Doublier, 2016) in the two-way time (TWT) domain. The brown structures are major crustal-scale faults penetrating the base of the crust. Only parts of these interpreted faults are displayed.